Broadband, Continuous-Wave, Mid-Infrared Generation Based on TFBG Spectral Modulation

Kaifeng Wang, Xiao Li, Peng Wang, Meng Wang, Weihong Hua, Zefeng Wang, and Kai Han

***Abstract*—We demonstrated a tilted fiber Bragg grating (TFBG)-based modulated amplified spontaneous emission (ASE) source, followed by the broadband, continuous-wave (CW) mid-infrared laser generated by intracavity difference-frequency generation (DFG). By flattening the spectrum of the ASE source during its power amplification and injecting another 1018 nm fiber laser in the optical parametric oscillation(OPO) cavity, nonlinear frequency conversion was achieved in the nonlinear crystal. By tuning the polarization period of the crystal, a three-peaked mid-infrared laser with a full width at half maximum (FWHM) of 130 nm and a four-peaked mid-infrared laser with an FWHM of 180 nm was generated.**

***Index Terms*—Spectral modulation, mid-infrared laser, nonlinear optics, fiber laser.**

I. Introduction

MID-infrared lasers play an important role in environmental monitoring, medical diagnosis, and military countermeasures [1], [2], [3], [4]. The nonlinear frequency conversion technique based on nonlinear crystal implementation is one of the effective methods to generate the mid-infrared laser. Compared with the typical single-peaked mid-infrared laser, the multi-peaked broadband mid-infrared laser generated by nonlinear frequency conversion plays an efficient role in measurement calibration and analysis [5], [6], [7].

The OPO spectral tuning techniques for generating broadband multi-peaked mid-infrared laser are divided into two methods. One is a particular phase-matching technique of the pump source: the broadband sources with particular point phase-matching [8] and non-collinear phase-matching [9] provide a fundamental basis for developing broadband mid-infrared laser. The other is by tuning the oscillator process to achieve broadband multi-peaked mid-infrared laser, the special nonlinear crystal [10], [11] and resonant cavity structure [12], [13], [14], [15] greatly enriched the generation methods of the mid-infrared laser. However, the broadband multi-peaked mid-infrared laser is mainly generated using a pulsed pump source. In CW systems, generating broadband or multi-peaked mid-infrared laser is challenging because the broadband phase-matching condition requires a large pumping bandwidth and a high pumping threshold.

The ASE fiber source is chosen as the pump source to generate the broadband CW mid-infrared laser because of its broadband spectrum and excellent spectral stability. In 2016, Y Shang et al. pumped OPO by an ASE source with an FWHM of 9 nm. A mid-infrared laser with an FWHM of 72 nm and a maximum power of 11.3 W was generated under phase-matching [16]. It can be found from comparing the spectrum that the intensity of the seed source in the short-wave direction is reduced more than that in the long-wave order during power amplification, and there is a subsequent phenomenon such as drift of the central wavelength. Therefore, if a particular method is used to suppress the intensity of the seed source in the long-wave direction and then amplify the power, the gain flattening of the ASE source in the amplified process can be achieved, thus realizing a broadband CW pump source, and the selection of the gain flattening filter is analyzed below.

With the maturity of fiber grating inscription technology in recent years, it has been widely used in fiber optic communication [17], [18] and fiber sensing [19], [20], [21], especially in the flatness of the gain and ASE suppression [22], [23], [24]. The TFBG is selected for the required flattening requirements and existing conditions. The TFBG has excellent gain flattening characteristics and mode coupling features, providing suitable conditions for implementing broadband pump sources.

In this work, the TFBG is used to modulate the spectrum of the ASE seed source during the power amplification, and finally, the ASE fiber source is flattened. The ASE source is injected into the OPO cavity in parallel with a narrow linewidth 1018 nm laser, and the signal beam generated by the OPO process of the 1018 nm laser is mixed with the ASE source in the OPO cavity by tuning the phase-mismatched polarization period of the MgO: periodically poled lithium niobate (PPLN). By nonlinear frequency conversion of the ASE source, the double-peaked idler beam under phase-mismatching and the three-peaked and four-peaked idler beam under convergence to phase-matching is finally obtained. The maximum FWHM of the three-peaked idler beam is 130 nm, and the maximum FWHM of the four-peaked idler beam is 180 nm, which is the widest three-peaked and four-peaked broadband mid-infrared laser generated by the CW

Manuscript received 25 July 2022; revised 25 August 2022; accepted 10 September 2022. Date of publication 14 September 2022; date of current version 28 October 2022. This work was supported by the National Natural Science Foundation of China under Grants 61975236 and 2019-JCJQ-JJ-202. *(Corresponding author: Xiao Li.)*

Kaifeng Wang, Xiao Li, Peng Wang, Meng Wang, Weihong Hua, Zefeng Wang, and Kai Han are with the College of Advanced Interdisciplinary Studies, National University of Defense Technology, Changsha 410073, China, with the Nanhu Laser Laboratory, National University of Defense Technology, Changsha 410073, China, and also with the Hunan Provincial Key Laboratory of High Energy Laser Technology, Changsha 410073, China (e-mail: wkfeng0123@163.com; crazy.li@163.com; 1169723259@qq.com; 451428207@qq.com; huawj@163.com; zefengwang_nudt@163.com; hankai0071@nudt.edu.cn).

Digital Object Identifier 10.1109/JPHOT.2022.3206429

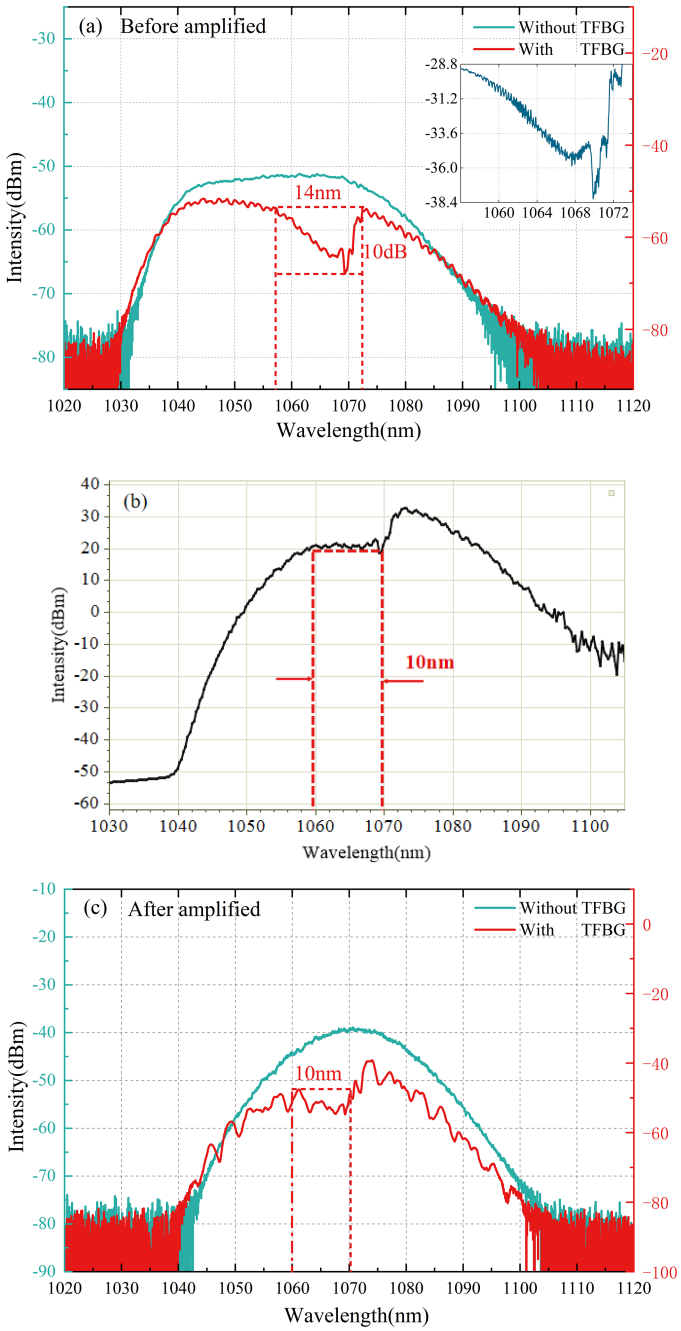

Fig. 1. **(a)** ASE seed source spectrum and spectrum after TFBG-modulation. The insert shows the transmission spectrum of TFBG2. **(b)** ASE source simulation spectrum. **(c)** ASE seed source spectrum after amplification and spectrum after TFBG-modulation and then amplification.

system. The stability and controllability of the idler spectrum during the modulation of nonlinear frequency conversion are further discussed.

II. Experimental Setup and Methods

Fig. 1(a) shows the spectrum before power amplification. The TFBG with transmission spectrum depth of 10 dB and bandwidth of 14 nm is used for gain suppression of the ASE seed source. The spectral evolution of the ASE source during power

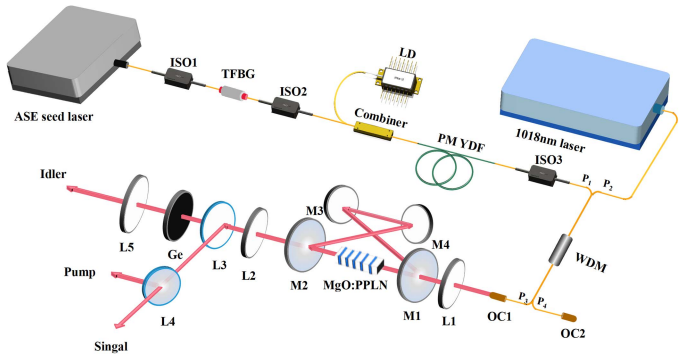

Fig. 2. Diagram of continuous-wave OPO experimental setup.

amplification is analyzed. The ytterbium (Yb)-doped fiber's absorption-emission spectrum is the first to split into multiple separated spectra at equal intervals. After that, the laser within it is viewed as a single wavelength, and a rate equation is established for it, which allows a better consideration of the effect of each wavelength on the total gain and the competition between the wavelengths, resulting in the ASE simulation spectrum plot shown in Fig. 1(b). The power-amplified spectrum is flatter at 1060–1070 nm, which meets the experimental requirements. Fig. 1(c) shows the spectrum after power amplification. During the experiment, it was found that the intensity suppression of the TFBG-modulated ASE source spectrum at 1070 nm was more evident after the power amplification. It was analyzed that the difference in the absorption-emission spectrum of Yb^{3+} in the gain fiber for different wavelengths of laser absorption coefficients led to the lower intensity of the ASE source at 1070 nm after power amplification.

The power of the ASE seed source after modulation is 70 mW, and the power reaches 2.5 W after power amplification. It can be seen that the power of the ASE source cannot get the oscillation threshold of the OPO process [9]. As a result of the above, this research uses intracavity DFG for nonlinear frequency conversion of ASE sources. The intracavity DFG can effectively reduce the pumping threshold in the nonlinear frequency conversion process, which provides an excellent solution to realize the nonlinear frequency conversion of the ASE source [25], [26].

The experimental structure is shown in Fig. 2. The 1018 nm laser generates a near-infrared signal beam by the OPO in the crystal. The ASE source first enters the cavity through a wavelength division multiplexer (WDM) with the 1018 nm laser and later generates a mid-infrared laser in the PPLN crystal with the signal beam. The maximum power of the 1018 nm laser is 46 W.

The ASE fiber source has a master oscillator power amplification (MOPA) structure. One is the main oscillator part of the seed source: The seed laser is a 1060 nm ASE source with an FWHM of 23 nm and a maximum power of 100 mW. It passes through the isolator (ISO1) and the TFBG to achieve preliminary spectral modulation. The power amplification includes a $(2 + 1) \times 1$ pump & signal combiner (PSC) and 11 m polarization-maintaining 10/125 μm Yb-doped optical fiber. A

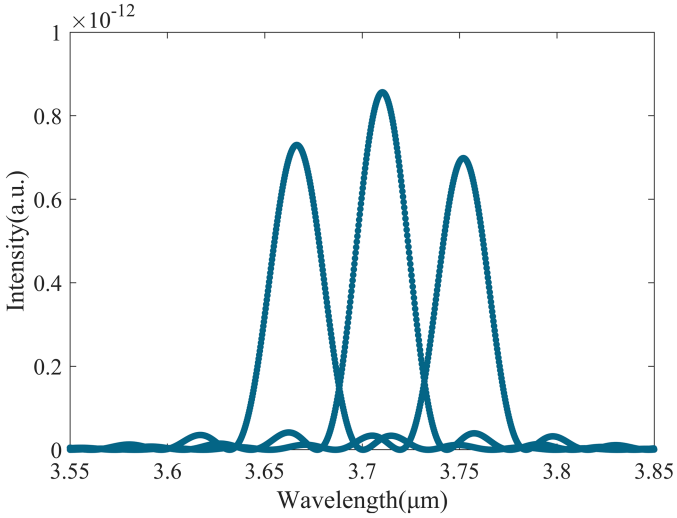

Fig. 3. Simulated idler spectrum.

915 nm laser diode (LD) with a maximum power of 50 W is fused with the pump arms of the PSC. After passing ISO2, the ASE source is connected with the 1018 nm laser with a 2 × 2 structure WDM (1018/1070 nm). Port 1 and 2 of the WDM are connected with two lasers, port 3 is connected with the OPO system, port 4 is connected with the optical collimator (OC2), and the spectral characteristics of the pump beam are detected by using a spectrometer. The PPLN crystal used for the OPO resonant cavity is a sector-periodic structure.

The OPO is a single resonant cavity: L1 and L2 are the cavity mirrors of the OPO; M1 and M2 are the curved mirrors inside the OPO cavity; M3 and M4 are flat mirrors. L3 (mid-infrared high transmission: 0.9∼1.8 μm) with a germanium (Ge) sheet is used to filter the pump beam and signal beam. The remaining pump beam and signal beam are separated by using L4 so that the power and spectrum of both can be monitored and recorded. At this time, there is an idler beam generated by the OPO of the 1018 nm laser in the mid-infrared generation, which is filtered by L5 (dichroic mirror: 2.7–3.1 μm high reflection, 3.6–3.9 μm high transmission), and the DFG idler beam is recorded for power and spectrum.

The signal beam and the ASE source are satisfied with the three-wave coupling equation, and the idler power satisfies the DFG efficiency equation [27].

$$\eta = \frac{p_i}{p_p} = \frac{4\omega_i^2 d_{eff}^2 k_s P_s}{\pi c^3 \varepsilon_0 n_p n_s n_i (1+\mu)} h(\mu,\xi)\sin c^2(\Delta k L/2) \quad (1)$$

P is the beam power, L is the crystal length, ω is the angular frequency, Δk is the phase-mismatching, d_{eff} is the effective nonlinear coefficient, k is the wave vector, c is the speed of light in vacuum, ε_0 is the free space permittivity, n is the refractive index, h(μ, ξ) is the focusing parameter, $\mu = k_s/k_p$, ξ = l/b, b $= 2\pi\omega^2 n/\lambda$ is called the confocal parameter. The pump spectral data are divided into separated spectra at equal intervals under phase-matching and brought into the equation.

Finally, the simulated spectrum is obtained. Fig. 3 shows that when the pump spectrum is flat at 1060–1070 nm, a three-peaked idler beam with FWHM up to 150 nm can be generated under phase-matching.

III. Experimental Results

As shown in Fig. 4, while tuning the sector crystal in the OPO cavity, the central wavelength of the DFG idler beam shifts from long-wave to short-wave direction as the phase-mismatching of the DFG process gradually decreases. The bandwidth of the idler beam has been broadened.

In Fig. 4(a), the wavelength of the central peak of the idler beam is located at 3748 nm, and the intensity difference between the central peak and the secondary peak is meager. The spectrum is bimodal with an FWHM of 50 nm. Due to the phase-mismatch, the bandwidth of the bimodal mid-infrared laser is far from the broadband standard, and the phase-mismatch needs to be further reduced. Fig. 4(b) shows an idler beam with the central wavelength of the central peak at 3732 nm, a bandwidth of 70 nm, and a secondary peak at 3762 nm. Eventually, with the tuning of the crystal period, when the phase-mismatching of the DFG process tends to 0, the idler beam at the central wavelength located at 3713 nm is three-peaked, as shown in Fig. 4(c), with an FWHM of 130 nm, where the central wavelengths at two secondary peaks are located at 3663 nm and 3764 nm, respectively.

The 1018 nm laser power is stabilized at 46 W. During the pumping power from 0.25 W to 2.5 W, the idler power is increased from 13 mW to 160 mW, and the pump-idler frequency conversion efficiency is 6.4%.

The central wavelength of each peak of the three-peaked idler beam is essentially matched in the experiment and simulation by comparing Fig. 4(c) with Fig. 3 but differs by 20 nm on the FWHM. In the DFG idler spectrum of Fig. 4(c), there is a low-intensity secondary peak at 3616 nm, and this peak has resulted in a reduction of the three-peaked idler bandwidth. However, the OPO cavity has reached the phase-matching state; either increasing the pump power or increasing the signal power can not improve the intensity of the secondary peak at 3616 nm, generating a four-peak idler beam, thus reaching the 150 nm bandwidth of the simulated idler spectrum. In the process of tuning the central wavelength of the multi-peaked idler beam gradually from 3713 nm to the short-wave direction, the four-peaked broadband idler beam is also not generated. The existence of this secondary peak demonstrates the feasibility of generating a four-peaked idler beam. Based on this, further thinking is needed on generating a four-peaked broadband idler beam.

The pump source has a low intensity at 1070 nm. Assuming that the depth of the transmission spectrum of the TFBG is reduced, whether the modulated and re-amplified laser can be a broadband or multi-peaked laser becomes an essential issue in generating a four-peaked broadband idler beam.

According to the analysis, the TFBG2 (depth: 3 dB, bandwidth: 9 nm) is customized and inserted into the ASE fiber source. The spectrum before power amplification and the amplified spectrum are shown in Fig. 5. The ASE source through the amplification is more similar to the shape of the spectrum

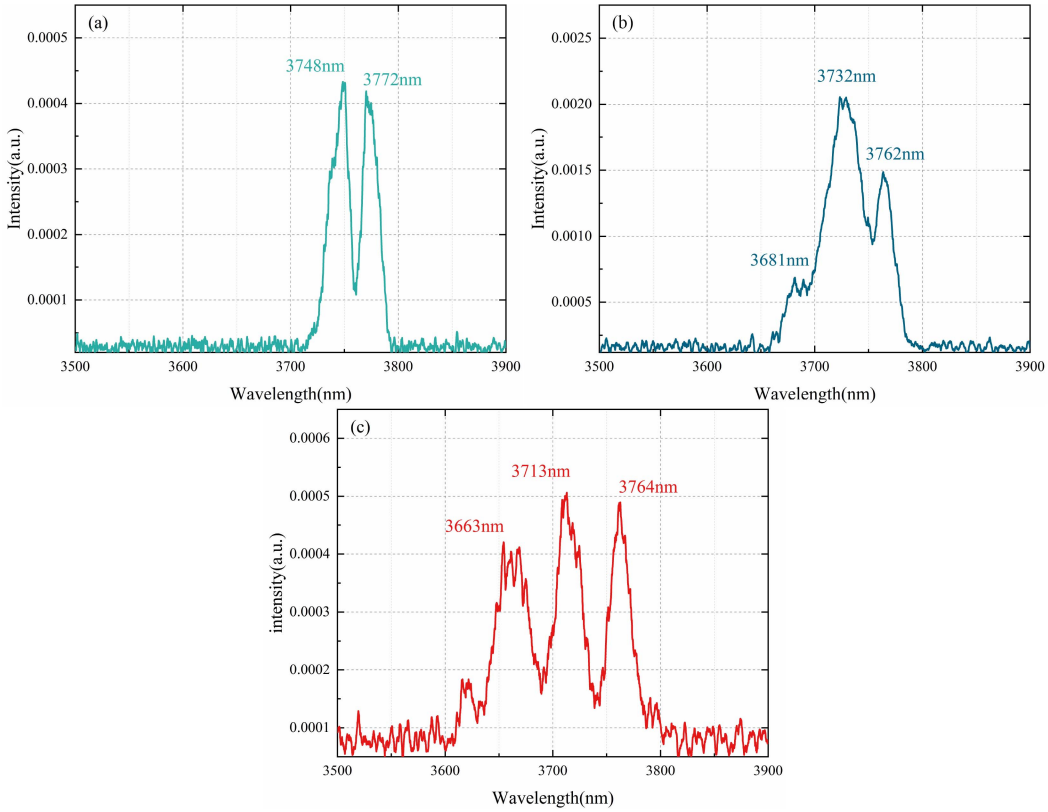

Fig. 4. Multi-peaked idler beam generated by the intracavity DFG at a TFBG transmission depth of 10 dB with FWHM of **(a)** 50 nm. **(b)** 70 nm. **(c)** 130 nm.

without TFBG2 but is more different from the ASE spectrum generated at the previous 10 dB depth. It is due to the lower transmission spectral depth of TFBG2, which results in different absorption of Yb^{3+} at each wavelength in the gain fiber. However, the overall absorption is similar to that without TFBG2.

The amplified ASE source spectrum has a gain flattening effect in the 1062 nm–1076 nm, and its injection into the OPO cavity as a pump laser will have a broadening impact on the bandwidth and crest of the generated idler beam.

As shown in Fig. 6(a), the central wavelength of the central peak is located at 3714 nm, the bandwidth of the three-peaked mid-infrared laser is 60 nm, and the wavelengths of the secondary peaks are located at 3679 nm and 3759 nm, respectively. A comparison of Fig. 6(a) with Fig. 5(c) shows that the wavelengths of the central peak of the generated three-peaked idler beams are similar, but the bandwidths are different. The pump source injected into the OPO is in phase-mismatching after accessing TFBG2, resulting in a lower intensity of the secondary peak than the central peak, affecting the idler bandwidth. The OPO cavity must be tuned closer to phase-matching.

At a pump power of 0.25 W, 1.7 W, and 2.5 W, the idler power is 11 mW, 70 mW, and 140 mW, and the pump-idler frequency conversion efficiency is 5.6%. Fig. 6(b) shows the spectrum of the four-peaked idler beam and the fitted curve, the central wavelengths of the four peaks of the idler beam are 3629 nm, 3669 nm, 3724 nm, and 3768 nm from short-wave to long-wave directions.

The ASE fiber source after TFBG modulation in Fig. 5(b) has four peaks in the flat range of 1062 nm–1076 nm, which are 1063.8 nm, 1067.2 nm, 1071.8 nm, and 1075.5 nm. In the intracavity DFG process, the pump beam, signal beam, and idler beam satisfy the three-wave coupling equation.

$$\frac{1}{\lambda_p} - \frac{1}{\lambda_s} = \frac{1}{\lambda_i} \tag{2}$$

λ is the central wavelength of the laser, and the subscripts p, s, and i represent the pump, signal, and idler beam. The 1018 nm laser generated a signal beam of 1505 nm through the OPO process. Under the same polarization period, calculated by the above equation, the central wavelengths of the four peaks of the generated DFG idler beam are 3629 nm, 3669 nm, 3724 nm, and 3768 nm, which also correspond to the central wavelengths of the four peaks of the four-peaked idler beam in Fig. 6(b). The broadband idler spectrum is broadened because of the modulation of the ASE source by TFBG2. The FWHMs of the four peaks are 22 nm, 27 nm, 39 nm, and 28 nm. Gauss function model fits the four-peaked DFG idler beams, the final fitted curve covers all areas of the four peaks, and the FWHM of the fitted curve reaches 180 nm. The idler beam with a bandwidth of 180 nm is the widest four-peaked broadband CW mid-infrared laser generated by nonlinear frequency conversion, in which the FWHM of the peaks ranges from 22 nm to 39 nm.

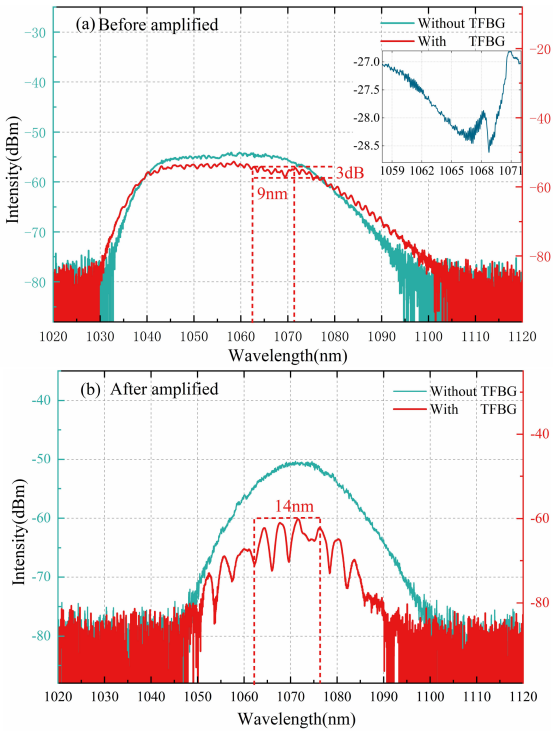

Fig. 5. **(a)** ASE seed source spectrum and spectrum after TFBG-modulation. The insert shows the transmission spectrum of TFBG2. **(b)** The amplified spectrum of ASE seed source and re-amplified spectrum after TFBG2 injection.

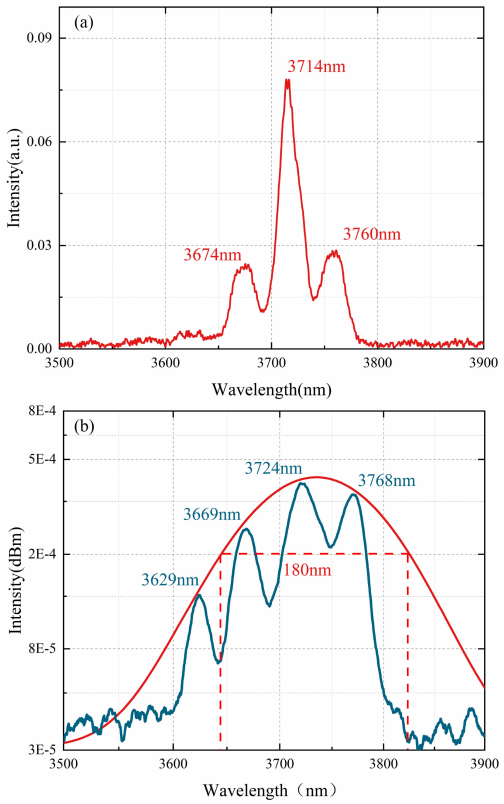

Fig. 6. **(a)** Three-peaked DFG idler spectrum. **(b)** The fitted curve of the four-peaked idler spectrum.

IV. Conclusion

In this research, gain flattening of an ASE fiber source during power amplification was achieved using TFBGs with different transmission spectral depths. The TFBG-based modulated ASE source was injected into the OPO cavity in parallel with a 1018 nm laser and a three-peaked and a four-peaked idler beam with a power of 0.16 W and 0.13 W were achieved by tuning the crystal polarization period at a pump power of 2.5 W. The FWHM of the three-peaked mid-infrared laser was 130 nm, and the FWHM of the four-peaked mid-infrared laser was 180 nm, which were the broadest three-peaked and four-peaked mid-infrared laser in the CW system. The bandwidth of each peak of the four-peaked mid-infrared laser was about 30 nm, which had rich practical application value and proved that the broadband pumping source with TFBG modulation had a good effect on the broadening of the idler beam with nonlinear frequency conversion.

Acknowledgment

The authors thank Nanjing University, Zhejiang University, and Fujian Institute of Research on the Structure for offering nonlinear crystals.

References

[1] T. Wu et al., "Compact hollow waveguide mid-infrared gas sensor for simultaneous measurements of ambient CO_2 and water vapor," *J. Lightw. Technol.*, vol. 38, no. 16, pp. 4580–4587, Aug. 2020.

[2] J. Yang, J. Zhou, and P. T. Lin, "Real-time isotopic methane detection using mid-infrared spectroscopy," *Appl. Opt.*, vol. 59, no. 34, pp. 10801–10807, Nov. 2020.

[3] M. Milanič, B. Majaron, and J. S. Nelson, "Spectral filtering for improved pulsed photothermal temperature profiling in agar tissue phantoms," *J. Biomed. Opt.*, vol. 13, no. 6, 2008, Art. no. 064002.

[4] Z. G. Figen, "Mid-infrared laser source for testing jamming code effectiveness in the field," *Opt. Eng.*, vol. 58, no. 08, Aug. 2019, Art. no. 086101.

[5] L. J. Olafsen and J. S. Olafsen, "Multi-wavelength beam profile analysis of near-infrared nanosecond pulses," *Infrared Phys. Technol.*, vol. 105, Mar. 2020, Art. no. 103228.

[6] D. Brida, M. Marangoni, C. Manzoni, S. D. Silvestri, and G. Cerullo, "Two-optical-cycle pulses in the mid-infrared from an optical parametric amplifier," *Opt. Lett.*, vol. 33, no. 24, pp. 2901–2903, Dec. 2008.

[7] Z. E. Loparo, E. Ninnemann, Q. Ru, K. L. Vodopyanov, and S. S. Vasu, "Broadband mid-infrared optical parametric oscillator for dynamic high-temperature multi-species measurements in reacting systems," *Opt. Lett.*, vol. 45, no. 2, pp. 491–494, Jan. 2020.

[8] R. Das, S. C. Kumar, G. K. Samanta, and M. Ebrahim-Zadeh, "Broadband, high-power, continuous-wave, mid-infrared source using extended phase-matching bandwidth in MgO:PPLN," *Opt. Lett.*, vol. 34, no. 24, pp. 3836–3838, Dec. 2009.

[9] J. Storteboom, C. J. Lee, A. F. Nieuwenhuis, I. D. Lindsay, and K.-J. Boller, "Incoherently pumped continuous wave optical parametric oscillator broadened by non-collinear phasematching," *Opt. Exp.*, vol. 19, no. 22, pp. 21786–21792, Oct. 2011.

[10] X. Wei et al., "Compact mid-infrared self-optical parametric oscillator directly-pumped by diode laser based on a single Nd: MgO: PPLN crystal," *Opt. Laser Technol.*, vol. 151, Jul. 2022, Art. no. 108062.

[11] S. Niu, P. Aierken, M. Ababaike, S. Wang, and T. Yusufu, "Widely tunable, high-energy, mid-infrared (2.2–4.8 μm) laser based on a multi-grating MgO: PPLN optical parametric oscillator," *Infrared Phys. Technol.*, vol. 104, Jan. 2020, Art. no. 103121.

[12] H. Huang, S. Wang, X. Liu, and D. Shen, "Simultaneous dual-wavelength nanosecond mid-infrared optical parametric oscillator," *Infrared Phys. Technol.*, vol. 93, pp. 91–95, Sep. 2018.

[13] G. Liu et al., "161 W middle infrared $ZnGeP_2$ MOPA system pumped by 300 W-class Ho: YAG MOPA system," *Opt. Lett.*, vol. 46, no. 1, pp. 82–85, Dec. 2020.

[14] G. K. Samanta, A. Aadhi, and M. Ebrahim-Zadeh, "Continuous-wave, two-crystal, singly-resonant optical parametric oscillator: Theory and experiment," *Opt. Exp.*, vol. 21, no. 8, pp. 9520–9540, Apr. 2013.

[15] H. Liu, Y. Yu, Y. Wang, L. Li, and G. Jin, "Multi-optical parametric oscillator based on electro-optical polarization mode conversion at 3.3 μm and 3.84 μm," *Infrared Phys. Technol.*, vol. 115, Jun. 2021, Art. no. 103702.

[16] Y. Shang, J. Xu, P. Wang, X. Li, P. Zhou, and X. Xu, "Ultra-stable high-power mid-infrared optical parametric oscillator pumped by a superfluorescent fiber source," *Opt. Exp.*, vol. 24, no. 19, pp. 21684–21692, Sep. 2016.

[17] A. F. Sayed, F. M. Mustafa, A. A. M. Khalaf, and M. H. Aly, "An enhanced WDM optical communication system using a cascaded fiber Bragg grating," *Opt. Quantum Electron.*, vol. 52, no. 3, Mar. 2020, Art. no. 181.

[18] G. Rego, P. Caldas, and O. V. Ivanov, "Arc-induced long-period fiber gratings at INESC TEC. Part II: Properties and applications in optical communications and sensing," *Sensors*, vol. 21, no. 17, Sep. 2021, Art. no. 5914.

[19] Y. Liu, A. Zhou, and L. Yuan, "Multifunctional fiber-optic sensor, based on helix structure and fiber Bragg gratings, for shape sensing," *Opt. Laser Technol.*, vol. 143, Nov. 2021, Art. no. 107327.

[20] J. A. Flores-Bravo, J. Madrigal, J. Zubia, S. Sales, and J. Villatoro, "Coupled-core fiber Bragg gratings for low-cost sensing," *Sci. Rep.*, vol. 12, no. 1, Jan. 2022, Art. no. 1280.

[21] T. Gang, X. Zhang, and R. Sun, "Tilted fiber Bragg grating fixed in a polypropylene tube for ultrasonic sensing and imaging of simulated geological models," *Opt. Laser Technol.*, vol. 140, Aug. 2021, Art. no. 107075.

[22] Y. Zheng et al., "108 kW spectral beam combination of eight all-fiber superfluorescent sources and their dispersion compensation," *Opt. Exp.*, vol. 24, no. 11, pp. 12063–12071, May 2016.

[23] W. Lin, M. Desjardins-Carrière, B. Sévigny, J. Magné, and M. Rochette, "Raman suppression within the gain fiber of high-power fiber lasers," *Appl. Opt.*, vol. 59, no. 31, pp. 9660–9666, Oct. 2020.

[24] C. Yang, Q. Zhao, Z. Feng, M. Peng, Z. Yang, and S. Xu, "1120 nm kHz-linewidth single-polarization single-frequency Yb-doped phosphate fiber laser," *Opt. Exp.*, vol. 24, no. 26, pp. 29794–29799, Dec. 2016.

[25] P. Wang, X. Cheng, X. Li, X. Xu, K. Han, and J. Chen, "Dual-wavelength mid-infrared generation using intracavity stimulated Raman scattering of PPLN," *IEEE Photon. J.*, vol. 10, no. 6, Dec. 2018, Art. no. 1504408.

[26] C. Xi, P. Wang, X. Li, and Z. Liu, "Highly efficient continuous-wave mid-infrared generation based on intracavity difference frequency mixing," *High Power Laser Sci. Eng.*, vol. 7, 2019, Art. no. 04000e67.

[27] T. Yanagawa, H. Kanbara, O. Tadanaga, M. Asobe, H. Suzuki, and J. Yumoto, "Broadband difference frequency generation around phase-match singularity," *Appl. Phys. Lett.*, vol. 86, no. 16, Apr. 2005, Art. no. 161106.